Inorganic Chemistry

ARTICLE

pubs.acs.org/IC

Interconversion between the Enantiomers of Chiral Five-Coordinate $Me_3Pt(IV)$ Complexes

Runyu Tan and Datong Song*

Davenport Chemical Research Laboratory, Department of Chemistry, University of Toronto, 80 St. George Street, Toronto, Ontario, Canada, M5S 3H6

Supporting Information

ABSTRACT: The dinuclear $Me_2Pt(II)$ complexes of 3,4-bis(quinolin-8-yl)thiophene (**1a**), 3,4-bis(6 trifluoromethoxyquinolin-8-yl)thiophene (**1b**), and 3,4-bis(2-methylquinolin-8-yl) thiophene (**1c**) react with MeOTf (OTf = trifluoromethanesulfonate) to afford the corresponding chiral mononuclear five-coordinate $Me_3Pt(IV)$ complexes $[PtMe_3(\mathbf{1a})]OTf$ (**3a**), $[PtMe_3(\mathbf{1b})]OTf$ (**3b**), and $[PtMe_3(\mathbf{1c})]OTf$ (**3c**), respectively. $[PtMe_3(\mathbf{1c})]BAr^F{}_4$ (**3d**) (where $BAr^F{}_4$ = $[B\{C_6H_3\text{-}3,5\text{-}(CF_3)_2\}_4]$) has also been synthesized for structural study. While **3a** appears to be symmetric in solution and asymmetric in solid state, **3c** and **3d** are asymmetric in both solution and solid state. The chirality originates from interligand repulsion, rather than any unsymmetrical ligand. Variable-temperature NMR and computational studies suggest a ligand-twisting isomerization pathway for the interconversion of the enantiomers, rather than the rotational exchange of three CH_3 ligands on the metal center.

INTRODUCTION

Five-coordinate Pt(IV) alkyl species have been proposed as key intermediates in oxidative addition and reductive elimination processes of Pt(II)/Pt(IV) chemistry.[1−5] The isolation of well-defined species of this type remains scarce. To date, only a few five-coordinate Pt(IV) alkyl species have been isolated by Goldberg,[6−10] Tilley,[11,12] and Wang.[13,14] As analogues, a handful of five-coordinate Pt(IV) silylhydride species have also been reported.[12,15−17] Most known examples involve an anionic bidentate ligand with nitrogen donor atoms; only $[Pt(BAB)Me_3]OTf$ (where BAB = 1,2-bis(*N*-7-azaindolyl)benzene and OTf = trifluoromethanesulfonate or triflate) by Wang involves a neutral bidentate BAB ligand,[13] the phenyl group of which is able to block the sixth coordination site of the metal center and phenyl group itself cannot act as the sixth ligand due to the large distance between the phenyl group and Pt (3.18 Å revealed by X-ray crystallography). In all the reported five-coordinate $Me_3Pt(IV)$ complexes, high solution-phase fluxionality was observed, and this behavior was generally attributed to the rotational exchange of Pt-CH_3 on NMR time scale (eq 1). For example, ^1H NMR spectra of complexes $[\{(o\text{-}^iPr_2C_6H_3)NC(CH_3)\}_2CH]PtMe_3$ (**1**, see eq 1), $(AnIm)Pt(CH_3)_3$ (**2**, see eq 1), and $(DtBPP)PtMe_3$ (**3**, eq 1) showed only one Pt−Me resonance, indicating fast exchange of Pt-CH_3 groups in solution. ^1H NMR spectra of complex $(BAB)PtMe_3$ (**4**, eq 1) showed two broad Pt-CH_3 peaks at room temperature and a coalescence of the two peaks at elevated temperature, suggesting a slow exchange of the basal Pt-CH_3 groups and the apical Pt-CH_3 group.

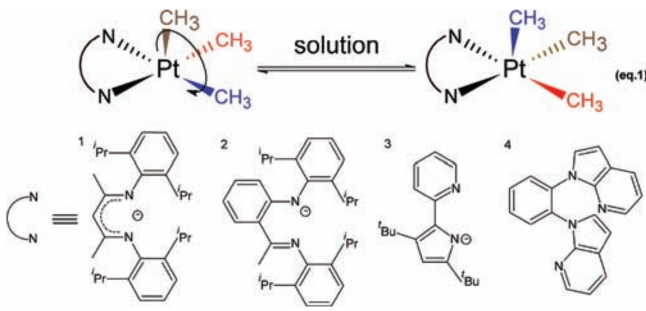

Previously, we reported a few quinoline-functionalized thiophene ligands, 3,4-bis(quinolin-8-yl)thiophene (**1a**) and 3,4-bis(6-trifluoromethoxyquinolin-8-yl)thiophene (**1b**), which enabled the isolation and full characterization of the first group 10 metal complexes of π-bound thiophenes.[18] Notably, the geometry of **1a** and **1b** is similar to that of Wang's BAB ligand, but the coordination mode displayed by **1a** and **1b** with $Me_2Pt(II)$ is very different from that of BAB (Chart 1, left), i.e., the *N,N*-chelation mode was not observed in **2a** or **2b** (the Me_2Pt complexes of **1a** and **1b**, respectively); rather, **2a** and **2b** feature the inverse sandwich dinuclear structure, with a quinoline nitrogen donor and a CC double bond of the thiophene ring bound to each Pt(II) center (Chart 1, right). This structural difference could be attributed to the better π-accepting ability and lower aromaticity of a thiophene ring, compared to a benzene ring. Although the structures of **2a** and **2b** differ much from that of $[PtMe_2(BAB)]$, some common features do exist, e.g., one side of the Pt(II)

Received: April 27, 2011
Published: October 12, 2011

Chart 1

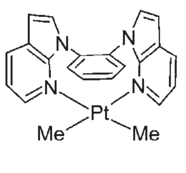

[Pt(BAB)Me_2]

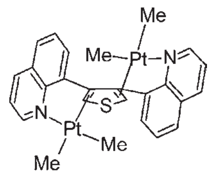

2a

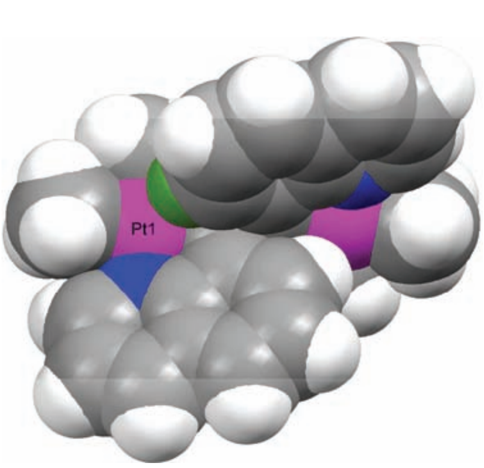

Figure 1. Space-filling model of the structure of **2a**, showing that one side of the Pt1 coordination plane is partially blocked by the hydrogen atom highlighted in green.

coordination plane is blocked by the chelating ligand. In the case of [$PtMe_2$(BAB)], it is the phenylene linker that blocks one side of the Pt(II) coordination plane, while in **2a** and **2b**, it is the C−H bond of an adjacent quinoline ring that partially blocks one side of the Pt(II) coordination plane (see Figure 1). Such partial blockage prompted us to study the oxidation of **2a** and **2b**, hoping to obtain dinuclear complexes of five-coordinate Pt(IV)Me_3. To our surprise, mononuclear five-coordinate Pt(IV)Me_3 complexes, formulated as [$PtMe_3$(**1a**)]OTf (**3a**) and [$PtMe_3$(**1b**)]OTf (**3b**), were obtained instead. More interestingly, compound **3a** displays a chiral structure in the solid state.[19] These chiral five-coordinate complexes display a distinct type of solution behavior, compared to the related literature compounds. Both experimental and computational results are presented herein.

EXPERIMENTAL SECTION

General. Unless otherwise stated, all preparations and manipulations were performed in air and all reagents were purchased from commercial sources and used without further purifications. [$Pt(CH_3)_2(SMe_2)]_2$,[20] 2-methyl-8-quinolineboronic acid,[21] 3,4-bis(quinolin-8-yl)thiophene (**1a**), 3,4-bis(6-trifluoromethoxyl-quinolin-8-yl)thiophene (**1b**), [Pt_2Me_4(1a)] (**2a**), and [Pt_2Me_4(1b)] (**2b**) were prepared according to the literature procedures.[18] NMR spectra were recorded on a Varian 400 spectrometer, or a Bruker Avance 400 spectrometer. Both ^{1}H and ^{13}C NMR spectra were referenced relative to the solvent's residual signals but are reported relative to Me_4Si. Elemental analyses were performed in the Chemistry Department at the University of Toronto with a Model PE 2400 C/H/N/S analyzer (Perkin−Elmer).

Synthesis of 3,4-bis(2-methyl-quinolin-8-yl)thiophene (1c). A mixture of $Pd(PPh_3)_4$ (115 mg, 0.1 mmol), 3,4-dibromothiophene (240 mg, 1.0 mmol), 2-methyl-8-quinolineboronic acid (512 mg, 3.0 mmol), and K_3PO_4 (1.9 g, 9.0 mmol) was placed in a Schlenk flask under argon. Degassed DMF (8 mL) and H_2O (4.5 mL) was added to the mixture and the flask was heated at 90 °C under argon for 24 h. The mixture was then cooled and partitioned by CH_2Cl_2 and water, and the organic layer was washed with water several times. The aqueous layers were combined together and washed with a small amount of CH_2Cl_2. The organic layers were then combined, washed with brine, and dried over $MgSO_4$. After filtration, the solvent was removed under vacuum, and the crude product was purified through a silica gel column using EtOAc/hexanes as an eluent and recrystallized from CH_2Cl_2/hexanes to afford **1c** as colorless crystals (135 mg, 40% yield). ^{1}H NMR ($CDCl_3$, 400 MHz, 25 °C): δ 7.78 (d, ^3J = 8.0 Hz, 2H), 7.65 (s, 2H), 7.51 (dd, ^3J = 8.0 Hz, ^4J = 1.2 Hz, 2H), 7.47 (dd, ^3J = 8.0 Hz, ^4J = 1.2 Hz, 2H), 7.21 (t, ^3J = 8.0 Hz, 2H), 6.95 (d, ^3J = 8.0 Hz, 2H), 2.23 (s, 6H). ^{13}C NMR ($CDCl_3$, 100 MHz, 25 °C): δ 157.8, 145.3, 141.1, 136.5, 135.5, 130.5, 126.4, 126.3, 125.0, 124.8, 121.2, 24.8. Anal. Calcd. for $C_{24}H_{18}N_2OS \cdot {}^1/_2CH_2Cl_2$: C, 71.96; H, 4.68; N 6.85. Found: C, 71.56; H, 4.96; N, 7.33.

Synthesis of [Pt_2Me_4(1c)] (2c). **1c** (32 mg, 0.059 mmol) and $[Pt(CH_3)_2(SMe_2)]_2$ (35 mg, 0.06 mmol) were dissolved in 3 mL of benzene, and the mixture was stirred for 2 h at ambient temperature. The solvent was removed under reduced pressure and the residue was recrystallized from benzene/hexanes to afford **2c** as pale-yellow crystals (56 mg, 95% yield). ^{1}H NMR ($CDCl_3$, 400 MHz, 25 °C): δ 8.75 (d, ^3J = 8.0 Hz, 2H), 8.17 (d, ^3J = 8.0 Hz, 2H), 7.54 (d, ^3J = 8.0 Hz, 2H), 7.44 (d, ^3J = 8.0 Hz, 2H), 7.28 (t, ^3J = 8.0 Hz, 2H), 5.77 (s, satellite, $^2J_{Pt-H}$ = 50.0 Hz, 2H), 2.97 (s, 6H), 1.04 (s, satellite, $^2J_{Pt-H}$ = 88.8 Hz, 6H), −0.24 (s, satellite, $^2J_{Pt-H}$ = 80.8 Hz, 6H). $^{13}C\{^1H\}$ NMR ($CDCl_3$, 100 MHz, 25 °C): δ 160.0, 148.6, 136.8, 136.4, 131.3, 127.8, 126.6, 125.3, 124.1, 104.1, 90.9, 26.5, 4.2, −9.1. Anal. Calcd for $C_{28}H_{30}N_2SPt_2 \cdot {}^1/_4C_6H_6$: C, 42.37; H, 3.79; N 3.35. Found: C, 41.99; H, 4.11; N, 2.79.

Synthesis of [$PtMe_3$(1a)]OTf (3a). **2a** (10 mg, 0.01 mmol) and **1a** (5 mg, 0.01 mmol) were dissolved in 2 mL of dichloromethane, and MeOTf (2.19 μL, 0.02 mmol) was added into this solution. The mixture was stirred for 3 h at ambient temperature, and the solvent was removed under reduced pressure. The crude product was recrystallized by vapor diffusion of pentane into THF/DCM solution to afford **3a** as colorless crystals (yield 75%). ^{1}H NMR (CD_2Cl_2, 400 MHz, 25 °C): δ 8.47 (dd, ^3J = 4.8 Hz, ^4J = 1.6 Hz, 2H), 8.35 (dd, ^3J = 8.4 Hz, ^4J = 1.6 Hz, 2H), 7.84 (s, 2H), 7.79 (dd, ^3J = 6.8 Hz, ^3J = 2.8 Hz, 2H), 7.52 (dd, ^3J = 8.4 Hz, ^3J = 2.8 Hz, 2H), 7.48−7.44 (m, 4H), 1.65 (s, satellite, $^2J_{Pt-H}$ = 76.8 Hz, 3H), 0.53 (s, satellite, $^2J_{Pt-H}$ = 67.6 Hz, 6H). $^{13}C\{^1H\}$ NMR (CD_2Cl_2, 100 MHz, 25 °C): δ 150.5, 146.5, 140.8, 136.5, 133.6, 131.7, 130.9, 130.5, 129.8, 128.1, 123.4, 13.6, −3.7 (CF_3 carbon was not observed). ^{19}F (CD_2Cl_2, 376 MHz, 25 °C): δ −78.84. Anal. Calcd for $C_{26}H_{23}N_2O_3F_3S_2Pt \cdot {}^1/_2THF$: C, 44.03; H, 3.56; N 3.67. Found: C, 43.85; H, 3.65; N, 3.65.

Synthesis of [$PtMe_3$(1b)]OTf (3b). The same procedure as above was used, using **2b** and **1b** as the starting material (yellow oil, yield 85%). ^{1}H NMR ($CDCl_3$, 400 MHz, 25 °C): δ 8.86 (dd, ^3J = 4.8 Hz, ^4J = 1.6 Hz, 2H), 8.38 (dd, ^3J = 8.4 Hz, ^4J = 1.6 Hz, 2H), 7.96 (s, 2H), 7.88 (dd, ^3J = 8.0 Hz, ^3J = 4.0 Hz, 2H), 7.66 (d, ^4J = 1.2 Hz, 2H), 7.31 (d, ^4J = 2.0 Hz, 2H), 1.89 (s, satellite, $^2J_{Pt-H}$ = 76.8 Hz, 3H), 0.61 (s, satellite, $^2J_{Pt-H}$ = 67.6 Hz, 6H). $^{13}C\{^1H\}$ NMR (CD_2Cl_2, 100 MHz, 25 °C): δ 151.4, 147.3, 144.6, 140.8, 137.5, 135.0, 133.1, 131.0, 130.2, 124.8, 119.2, 14.1, −3.4 (CF_3 carbons were not observed). ^{19}F ($CDCl_3$, 376 MHz, 25 °C): δ −78.14 (s, 3F), −58.13 (s, 6F). ESI-MS: calcd for $C_{27}H_{21}F_6N_2O_2PtS$: 746.03; found: 746.03 $[M]^+$.

Table 1. Crystallographic Data

	1c·$^1/_2$CH$_2$Cl$_2$	2c·C$_6$H$_6$	3a·$^1/_2$THF	3d
formula	$C_{24}H_{18}ClN_2S$	$C_{34}H_{36}N_2Pt_2S$	$C_{28}H_{27}F_3N_2O_{3.5}PtS_2$	$C_{59}H_{39}BF_{24}N_2PtS$
formula weight, FW	408.93	894.89	763.73	1469.88
temperature, T (K)	150(2)	150(2)	150(2)	150(2)
space group	C2/c	C2/c	$P2_12_12$	$P2_1/n$
unit-cell parameters				
a (Å)	18.9127(5)	36.6641(14)	12.0881(8)	21.8015(7)
b (Å)	12.0454(3)	9.8077(4)	24.2781(15)	12.8443(4)
c (Å)	18.9174(5)	19.2256(8)	9.4344(4)	22.2233(7)
α (deg)	90	90	90	90
β (deg)	113.3960(10)	119.9230(10)	90	114.1690(10)
γ (deg)	90	90	90	90
volume, V (Å^3)	3955.27(18)	5991.8(4)	2768.8(3)	5677.6(3)
Z	8	8	2	4
density, D_c (g cm^{-3})	1.373	1.984	1.832	1.720
μ (mm^{-1})	0.312	9.424	5.275	2.629
no. reflns collcd	17629	25433	13502	50524
no. indept reflns	4915	6538	6305	13060
goodness of fit (GOF) on F^2	1.047	1.129	1.039	1.021
R [$I > 2\sigma$ (I)]	R_1 = 0.0415	R_1 = 0.0274	R_1 = 0.0388	R_1 = 0.0632
	wR_2 = 0.0978	wR_2 = 0.0646	wR_2 = 0.0869	wR_2 = 0.1487
R (all data)	R_1 = 0.0612	R_1 = 0.0314	R_1 = 0.0526	R_1 = 0.0978
	wR_2 = 0.1075	wR_2 = 0.0663	wR_2 = 0.1005	wR_2 = 0.1658

Scheme 1. Syntheses of 3a and 3b

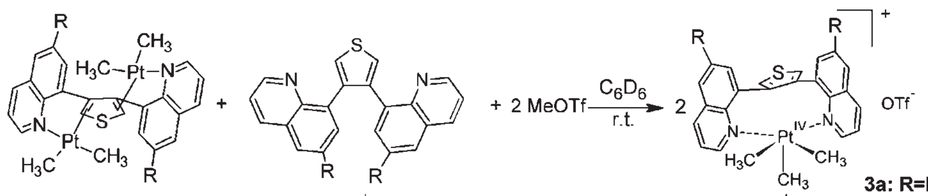

2a: R=H

2b: R=OCF$_3$

3a: R=H

3b: R=OCF$_3$

Synthesis of [PtMe$_3$(1c)]OTf (3c). The same procedure as above was used, using **2c** and **1c** as the starting material (white solid, yield 90%). ^{1}H NMR (CDCl$_3$, 400 MHz, 25 °C): δ 8.48 (d, ^3J = 8.0 Hz, 1H), 8.17 (dd, ^3J = 8.0 Hz, ^4J = 1.2 Hz, 1H), 8.11 (d, ^3J = 8.0 Hz, 1H), 7.97 (d, ^4J = 4.0 Hz, 1H), 7.91 (d, ^4J = 4.0 Hz, 1H), 7.88 (s, 1H), 7.77−7.73 (m, 2H), 7.67 (dd, ^3J = 8.0 Hz, ^4J = 1.2 Hz, 1H), 7.15−7.08 (m, 2H), 6.67 (dd, ^3J = 8.0 Hz, ^4J = 1.2 Hz, 1H), 3.00 (s, 3H), 1.60 (s, satellite, $^2J_{Pt-H}$ = 80.0 Hz, 3H), 1.49 (s, 3H), 1.06 (s, satellite, $^2J_{Pt-H}$ = 70.4 Hz, 3H), 0.25 (s, satellite, $^2J_{Pt-H}$ = 66.8 Hz, 3H). ^{13}C{^{1}H} NMR (CDCl$_3$, 100 MHz, 25 °C): δ 163.9, 163.7, 145.1, 144.7, 144.0, 141.7, 140.5, 140.2, 134.9, 133.5, 130.7, 130.5, 129.2, 128.6, 128.1, 128.0, 127.5, 127.0, 126.8, 126.3, 125.2, 122.8, 25.1, 25.0, 8.3, 0.1, −1.0 (CF$_3$ carbon was not observed). Anal. Calcd for $C_{28}H_{27}N_2O_3F_3S_2Pt \cdot {}^1/_3$THF: C, 45.18; H, 3.83; N 3.59. Found: C, 44.99; H, 4.28; N, 3.33.

Synthesis of [PtMe$_3$(1c)]BAr$^F{}_4$ (3d). **3c** (22 mg, 0.029 mmol) and NaBAr$^F{}_4$ (27.6 mg, 0.029 mmol) were stirred in 5 mL of DCM at room temperature for 4 h, and then the solution was filtered and the solvent was removed *in vacuo*. The residue was recrystallized in benzene/pentane mixture to afford the product as colorless crystalline solids (95% yield). ^{1}H NMR (CD$_2$Cl$_2$, 400 MHz, 25 °C): δ 8.38 (d, ^3J = 8.4 Hz, 1H), 8.19 (dd, ^3J = 8.0 Hz, ^4J = 1.2 Hz, 1H), 8.10 (d, ^3J = 8.0 Hz, 1H), 7.99 (d, ^4J = 4.0 Hz, 1H), 7.90 (dd, ^3J = 8.0 Hz, ^4J = 1.2 Hz, 1H), 7.82 (d, ^4J = 4.0 Hz, 1H), 7.79−7.75 (m, 1H), 7.73 (s, 8H), 7.68−7.63 (m, 2H), 7.56 (s, 4H), 7.14−7.10 (m, 1H), 7.04 (d, ^3J = 8.0 Hz, 1H), 6.74 (dd, ^3J = 8.0 Hz, ^4J = 1.2 Hz, 1H), 2.98 (s, 3H), 1.61 (s, satellite, $^2J_{Pt-H}$ = 80.4 Hz, 3H), 1.46 (s, 3H), 1.06 (s, satellite, $^2J_{Pt-H}$ = 70.4 Hz, 3H), 0.30 (s, satellite, $^2J_{Pt-H}$ = 67.6 Hz, 3H). Anal. Calcd for $C_{59}H_{39}BN_2F_{24}SPt$: C, 48.21; H, 2.67; N 1.91. Found: C, 48.34; H, 2.77; N, 1.92.

X-ray Diffraction Analyses. X-ray quality crystals of **1c** were obtained by top-layering the CH$_2$Cl$_2$ solution with hexanes; those of **2c** were obtained by diffusing pentane into benzene/CH$_2$Cl$_2$ solution, and those of **3a** and **3d** were obtained by diffusing pentane into THF solution. All crystals were mounted on the tip of a MiTeGen Micro-Mount and the single-crystal X-ray diffraction data were collected on a Bruker Kappa Apex II diffractometer. All data were collected with graphite-monochromated Mo Kα radiation (λ = 0.71073 Å) at 150 K controlled by an Oxford Cryostream 700 series low-temperature system. (Crystallographic data are given in Table 1.) The diffraction data were processed with the Bruker Apex 2 software package.[22] All structures were solved by direct methods and refined using SHELXTL V7.00.[23] Compound **1c** crystallized in the monoclinic space group

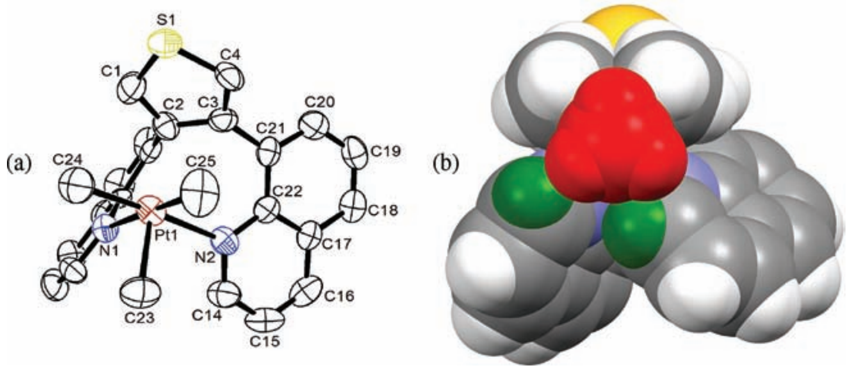

Figure 2. (a) Molecular structure of **3a** with thermal ellipsoids plotted at 50% probability; all hydrogen atoms and OTf^- are omitted for clarity. (b) Space-filling model (projection down the C23−Pt1 vector), showing the short contact between the apical Pt-methyl (red) and the quinoline protons (green).

Table 2. Selected Bond Lengths and Angles

Bond Lengths					
2c		**3a**		**3d**	
bond pairing	bond length (Å)	bond pairing	bond length (Å)	bond pairing	bond length (Å)
Pt(1)−C(27)	2.059(6)	Pt(1)−C(23)	2.041(7)	Pt(1)−C(25)	2.043(8)
Pt(1)−C(28)	2.041(5)	Pt(1)−C(24)	2.067(8)	Pt(1)−C(26)	2.043(8)
Pt(1)−N(2)	2.143(4)	Pt(1)−C(25)	2.036(8)	Pt(1)−C(27)	2.053(8)
Pt(1)−C(2)	2.238(5)	Pt(1)−N(1)	2.265(6)	Pt(1)−N(1)	2.276(5)
Pt(1)−C(1)	2.248(5)	Pt(1)−N(2)	2.162(6)	Pt(1)−N(2)	2.285(6)
C(1)−C(2)	1.421(7)	C(1)−C(2)	1.389(10)	C(1)−C(2)	1.409(11)
		C(2)−C(3)	1.365(10)	C(2)−C(3)	1.350(11)
		S(1)−C(1)	1.680(9)	S(1)−C(1)	1.685(8)
		S(1)−C(4)	1.712(9)	S(1)−C(4)	1.690(9)

Bond Angles					
2c		**3a**		**3d**	
bond angle	value (deg)	bond angle	value (deg)	bond angle	value (deg)
C(27)−Pt(1)−C(28)	84.4(4)	C(25)−Pt(1)−C(23)	87.8(4)	C(26)−Pt(1)−C(25)	88.7(4)
C(27)−Pt(1)−N(2)	94.8(2)	C(25)−Pt(1)−C(24)	86.0(4)	C(26)−Pt(1)−C(27)	85.5(4)
C(28)−Pt(1)−N(2)	175.8(2)	C(23)−Pt(1)−C(24)	82.1(4)	C(25)−Pt(1)−C(27)	81.1(4)
C(27)−Pt(1)−C(2)	165.7(2)	C(25)−Pt(1)−N(2)	92.7(3)	C(26)−Pt(1)−N(1)	173.7(3)
C(28)−Pt(1)−C(2)	100.7(2)	C(23)−Pt(1)−N(2)	179.3(3)	C(25)−Pt(1)−N(1)	94.1(3)
N(2)−Pt(1)−C(2)	80.99(18)	C(24)−Pt(1)−N(2)	97.5(3)	C(27)−Pt(1)−N(1)	89.3(3)
C(27)−Pt(1)−C(1)	155.8(2)	C(25)−Pt(1)−N(1)	176.1(3)	C(26)−Pt(1)−N(2)	95.0(3)
C(28)−Pt(1)−C(1)	99.8(2)	C(23)−Pt(1)−N(1)	95.4(3)	C(25)−Pt(1)−N(2)	100.0(3)
N(2)−Pt(1)−C(1)	79.23(17)	C(24)−Pt(1)−N(1)	92.4(3)	C(27)−Pt(1)−N(2)	178.8(3)
C(2)−Pt(1)−C(1)	36.95(18)	N(1)−Pt(1)−N(2)	84.0(2)	N(1)−Pt(1)−N(2)	90.1(2)

$C2/c$, with one molecule per asymmetric unit along with one-half molecule of dichloromethane. **2c** crystallized in the monoclinic space group $C2/c$, with one molecule per asymmetric unit along with one benzene molecule. **3a** crystallized in the orthorhombic space group $P2_12_12$ with one molecule per asymmetric unit along with one-half molecule of THF. Note: although the bulk sample of **3a** cannot be enantio-pure, the crystal we picked happened to be enantio-pure. **3d** crystallized in the monoclinic space group $P2_1/n$ with one molecule per asymmetric unit. The disordered benzene molecule in the lattice of **2c**, the OTf^- counterion of **3a**, and $BAr^F_4{}^-$ have been modeled successfully. All non-hydrogen atoms were refined anisotropically, except for those involved in the disordered portions. In all structures, hydrogen atoms bonded to carbon atoms were included in calculated positions and treated as riding atoms.

DFT Calculations. All calculations were performed using the Gaussian 09 software package[24] and the B3LYP method.[25,26] Platinum was treated with the lanl2dz basis set with effective core potential, while other elements were treated with a 6-31G* basis set. All structures were optimized in the gas phase. Vibrational frequency analyses were performed on all optimized structures to obtain thermodynamic data.

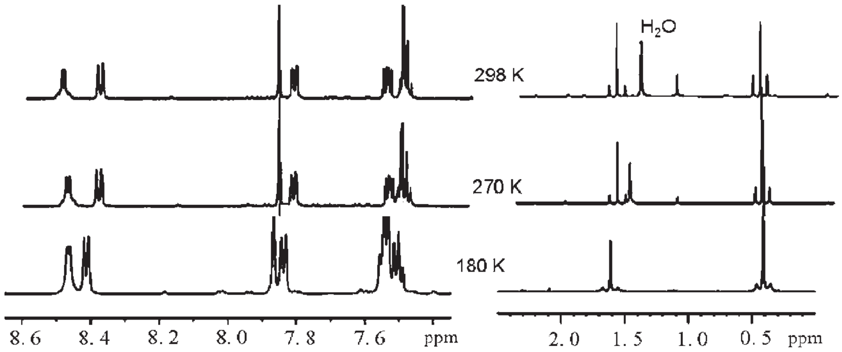

Figure 3. Low-temperature ^{1}H NMR spectra of **3a** (CD_2Cl_2, 400 MHz).

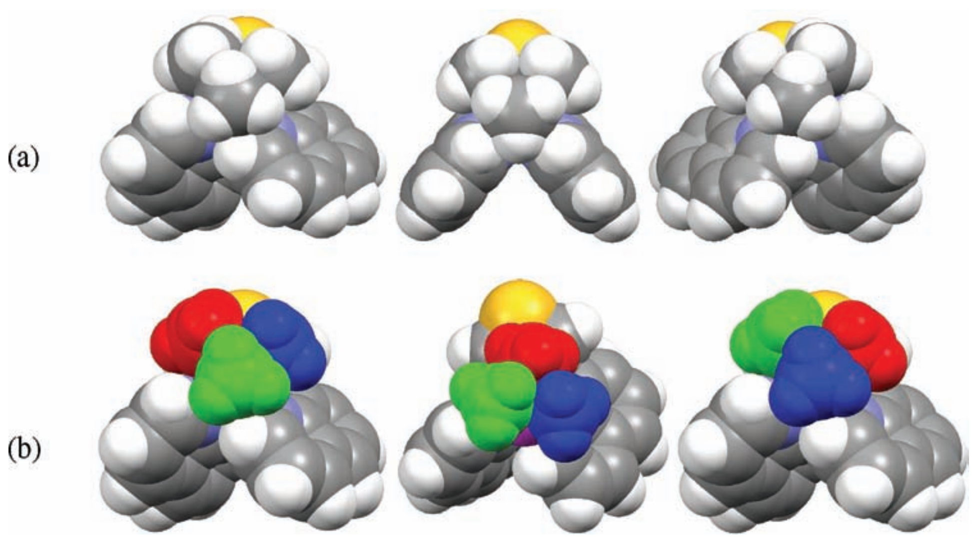

Figure 4. (a) Calculated interconversion pathway via ligand twisting: optimized structures of one enantiomer of **3a** (left), C_s symmetric transition state (middle), and the other enatiomer of **3a** (right). (b) Calculated pathway of rotational exchange of three methyl ligands: optimized structure of **3a** (left), transition state (middle), rotation product (right). Note: pathway (b) does not change the chirality of **3a**; the three methyl ligands in pathway (b) are highlighted in red, green, and blue, to illustrate the rotational process. The OTf^- counterion was not included in the calculations.

The atomic coordinates and free energies of all three optimized structures are listed in the Supporting Information.

■ RESULTS AND DISCUSSION

Synthesis and Characterization of Complex 3. It has been reported by Wang that [$PtMe_2$(BAB)] could react with 1 equiv of MeI to form $[PtMe_3I]_4$ and the free ligand BAB, because of the weak binding of BAB to Pt(IV)Me_3.[13] Interestingly, no reaction was observed between **2** and MeI after prolonged reaction time, even at elevated temperature. Since the oxidative addition of MeI typically occurs via an S_N2 fashion,[27] we reasoned that the partial blockage of one side of the Pt(II) coordination plane (Figure 1) could contribute to such inertness of **2** toward MeI. Also, the strong interaction between the Pt(II) and the CC double bonds of the thiophene may make the metal centers less nucleophilic, because of significant electron back-donation.[18]

To make the oxidation more favorable, a stronger oxidant (MeOTf) was then tested. MeOTf is broadly used as a strong methylating reagent and has proven extremely powerful in Pt(II)/Pt(IV) chemistry, thanks to the relatively noncoordinating property of the triflate anion. When complex **2a** is treated with 2 equiv of MeOTf, complete consumption of the starting materials can be observed within 2 h at ambient temperature. The resulting reaction mixture contains only $[Me_3PtOTf]_4$ (a singlet in the ^{1}H NMR spectrum at 1.50 ppm with $^{2}J_{Pt-H}$ of 82 Hz)[28] and a new species, **3a**. The stoichiometry of the reaction requires the formula of **3a** to be Me_3Pt(**2a**)OTf, which can also be produced from an independent reaction between **1a** and $[Me_3PtOTf]_4$ in a 4:1 molar ratio. Alternatively, **2a** can be cleanly transformed to **3a** by reacting with 1 equiv of **1a** and 2 equiv of MeOTf in one pot (see Scheme 1). At ambient temperature, the ^{1}H NMR spectrum of **3a** in CD_2Cl_2 shows two singlets with platinum satellites (apical methyl: 1.65 ppm, $^{2}J_{Pt-H}$ = 76.8 Hz; equatorial methyl ligands: 0.53 ppm, $^{2}J_{Pt-H}$ = 67.6 Hz) in the aliphatic region and only one set of quinolinyl and thiophene peaks in the aromatic region, indicating a symmetrical or fluxional structure in solution. ^{13}C NMR spectrum also supported the symmetrical/fluxional structure. The reaction of **3b** with MeOTf is similar to that of **3a**.

In contrast to the symmetric structure in solution disclosed by NMR spectroscopy, X-ray crystallography reveals an

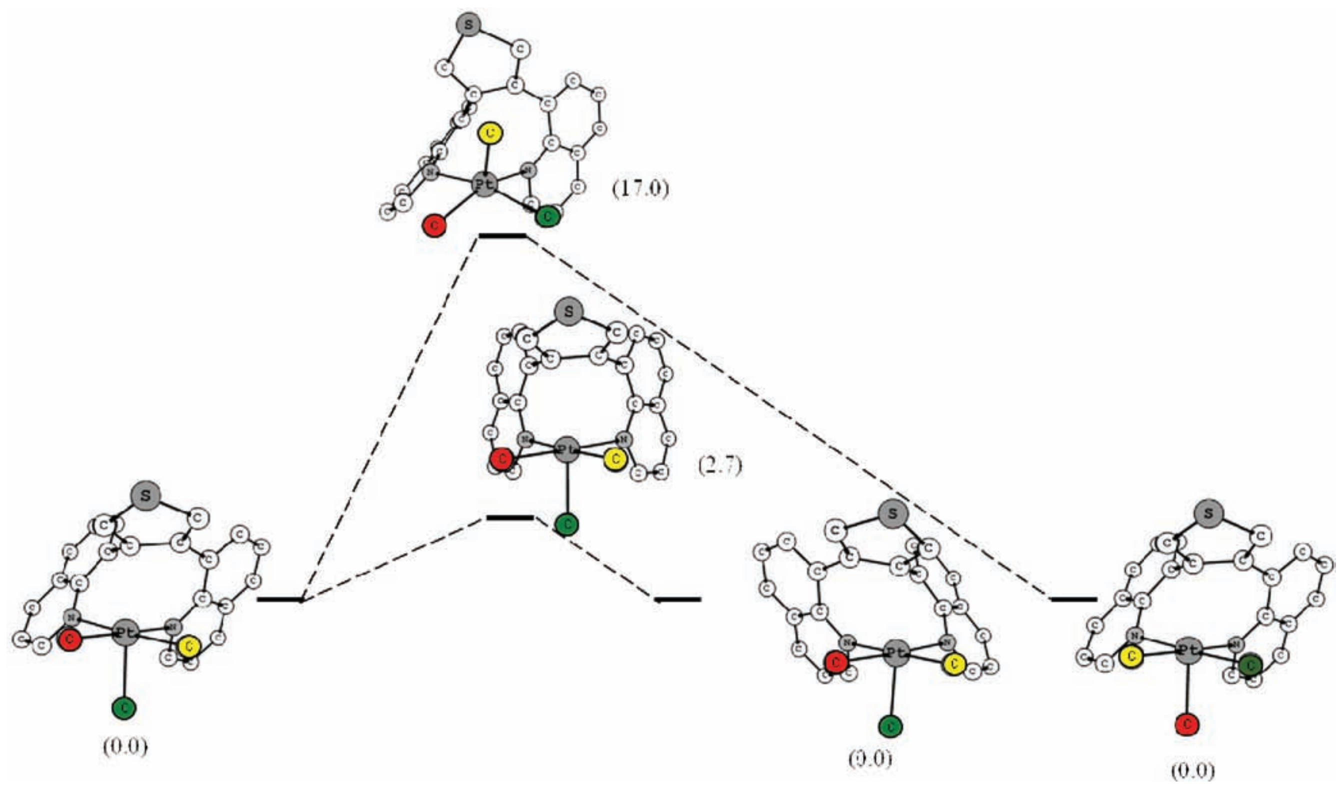

Figure 5. Energetics of the isomerization pathways of **3a**, relative to the free energy of the starting material (in kcal/mol, at 298 K). Methyl ligands are highlighted in different colors to illustrate the difference between the two processes. All the hydrogen atoms were omitted for clarity.

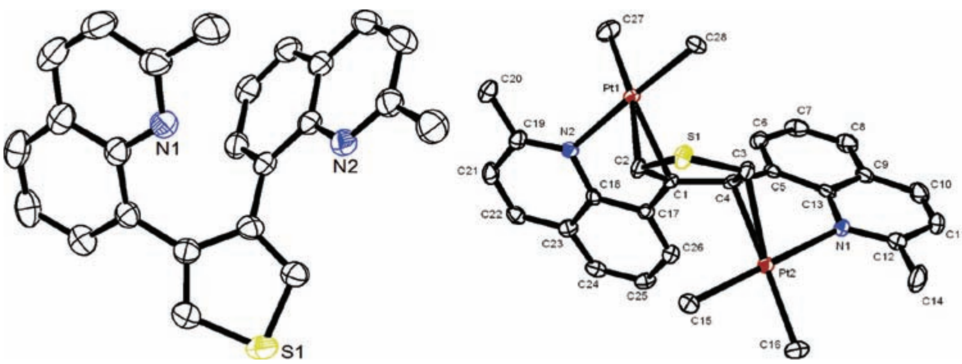

Figure 6. Molecular structure of **1c** (left) and **2c** (right) with thermal ellipsoids plotted at 50% probability; the solvent molecule and all the hydrogen atoms are omitted for clarity.

asymmetrical structure of **3a** in the solid state! As shown in Figure 2a, **3a** is a mononuclear five-coordinate Pt(IV) complex. Each cationic Pt center adopts a distorted square-pyramidal geometry, with two *cis* nitrogen donor atoms of the quinolinyl rings and two methyl ligands occupying the four basal coordination sites. The third methyl ligand is situated at the apical position. The C23−Pt1 vector points toward C2 of the thiophene ring: the distance between Pt1 and C2 (2.532(8) Å) is much shorter than that between Pt1 and C3 (2.932(7) Å). The two quinoline-to-thiophene dihedral angles are ~78.7° and ~49.8°, respectively. Accordingly, the Pt1−N1 and Pt1−N2 bond lengths are 2.265(6) and 2.162(6) Å, respectively, and the two basal Pt-methyl bond (Pt1−C24 and Pt1−C25) lengths are 2.067(8) and 2.036(8) Å, respectively. The apical Pt-methyl bond (Pt1−C23) length is 2.041(7) Å. Similarly, the bond lengths of Pt−C_{basal} and Pt−C_{apical} in five-coordinate Pt-Me_3 complexes reported by Wang[13] and Goldberg[6,9] are also statistically indistinguishable, likely due to the insignificant *trans* influence of the nitrogen donor atoms. (Selected bond lengths and bond angles for **2c**, **3a**, and **3d** are given in Table 2.) The crystal structure also shows that the apical methyl group is in short contact with two C−H bonds from the 2-positions of the quinoline rings (Figure 2b). It appears that the repulsion between the apical methyl ligand and the two quinoline C−H bonds prevents the formation of a C_s symmetric structure. The solution behavior of **3a** observed via NMR experiments is most likely the result of a fast interconversion of the two enantiomers, which involves twist around the C−C linkages between the thiophene ring and the quinoline rings (eq 2). This mechanism is reminiscent of the Ray−Dûtt twist observed in pseudo-octahedral complexes.[29]

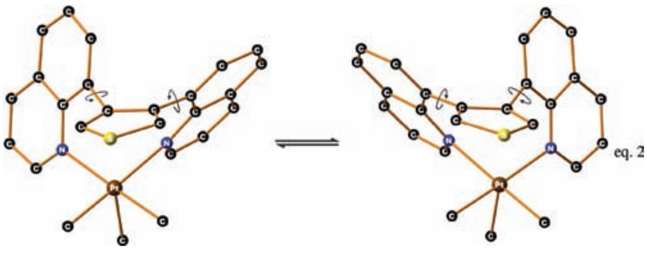

To measure the barrier of such an interconversion, we carried out variable-temperature NMR experiments. Unfortunately, the variable-temperature NMR experiments of **3a** (Figure 3) show that the interconversion process remains fast, even at 180 K in CD_2Cl_2 solution, as evidenced by only one set of quinoline signals and two singlet signals from the three methyl groups, suggesting a small energy barrier.

Computational Studies. Our computational studies reveal that the C_s conformation of **3a** is not a local minimum, but a saddle point on the energy surface, i.e., a transition state. The optimized structure of **3a** in C_s point group is shown in the middle of Figure 4a. The two quinoline C−H bonds are pointing directly at the apical methyl group on the Pt center, and any twist around the C−C linkages between the thiophene ring and the quinoline rings would lead to the observed chiral structure of **3a** and, thus, reduce the repulsions. The animated imaginary frequency indeed shows the twisting around the C−C linkages between the thiophene ring and the quinoline rings. The two enantiomers of **3a** can interconvert through the C_s symmetric transition state via the twisting motion. The calculated $\Delta G^{\ddagger}$ value for such an interconversion process is 2.7 kcal/mol (see Figure 5), which is consistent with the VT NMR study. The optimized ground- and transition-state structures are shown in Figure 4a.

To compare our proposed isomerization process with the rotational exchange of the three CH_3 ligands, we located the transition state of the rotational exchange process (Figure 4b). The calculated $\Delta G^{\ddagger}$ for the rotational exchange process is 17.0 kcal/mol (Figure 5), which is much higher than that of the interconversion of two enantiomers of **3a** and is inconsistent with our NMR results. Our calculations for the model species $[PtH_3(1a)]^+$, where the interligand repulsion is expected to be smaller than that of **3a**, also suggest a much smaller energy barrier for the ligand twisting mode (1.5 kcal/mol), compared to the rotational exchange mode (14 kcal/mol; see the Supporting Information).

Syntheses of 3c and 3d. Since the barrier of the interconversion of two enantiomers of **3a** is too small to measure using variable-temperature NMR, we sought to increase the barrier by creating more repulsion in the C_s symmetric transition state. As mentioned above, in the C_s conformation of **3a**, the C−H bonds at the 2-positions of the quinoline rings are pointing directly at the apical methyl group, causing interligand repulsions in the transition state. We envisioned that if the C−H bonds at 2-position of the quinoline rings are replaced with bulkier groups, e.g., introducing a methyl group at 2-position of the quinoline rings, greater repulsion could be achieved. To test our hypothesis, we synthesized ligand 3,4-bis(2-methylquinolin-8-yl)thiophene (**1c**), using the Suzuki coupling reaction (see Scheme 2). NMR spectra indicated a symmetric structure in solution, and the solid-state structure of **1c** was also confirmed by X-ray crystallography (see Figure 6, left). Similar to **1a** and **1b**, **1c** reacts with $[Pt_2Me_4(\mu\text{-}SMe_2)_2]$ to afford a dinuclear inverse sandwich complex $[Pt_2Me_4(\mathbf{1c})]$ (**2c**), whose structure has been confirmed with NMR spectroscopy and single-crystal X-ray diffraction (Figure 6, right). As shown in Figure 3, the installation of methyl groups on the quinoline rings did not significantly alter the coordination geometry of the Pt(II) centers, compared to that of **2a** and **2b**, and, consequently, did not impose a dramatic impact on the reactivity of **2c** toward MeOTf. Thus, compound **2c** reacts with 1 equiv of **1c** and 2 equiv of MeOTf in one pot, producing the corresponding Pt(IV) complex formulated as $[PtMe_3(\mathbf{1c})]OTf$ (**3c**). Alternatively, **3c** can also be prepared

Scheme 2. Synthesis of 1c

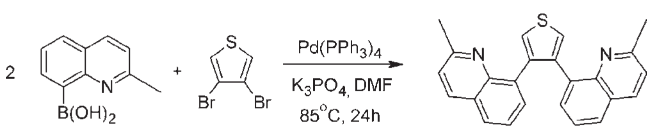

1c

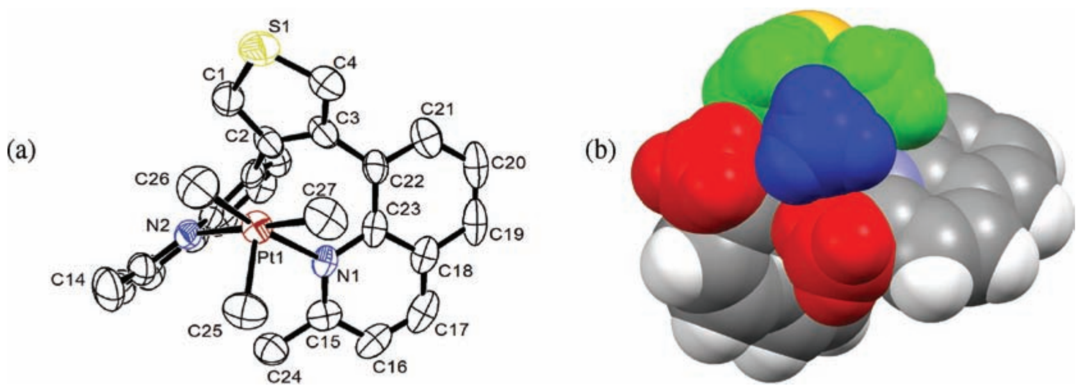

Figure 7. (a) Molecular structure of **3d** with thermal ellipsoids plotted at 50% probability; all hydrogen atoms and $BAr^F{}_4$ are omitted for clarity. (b) Space-filling model (projection down the C25−Pt1 vector) showing the short contact between the Pt-methyl groups and the quinoline methyl groups (basal Pt-methyl groups are highlighted in green, apical Pt-methyl are given in blue, and quinoline-methyl groups are shown in red).

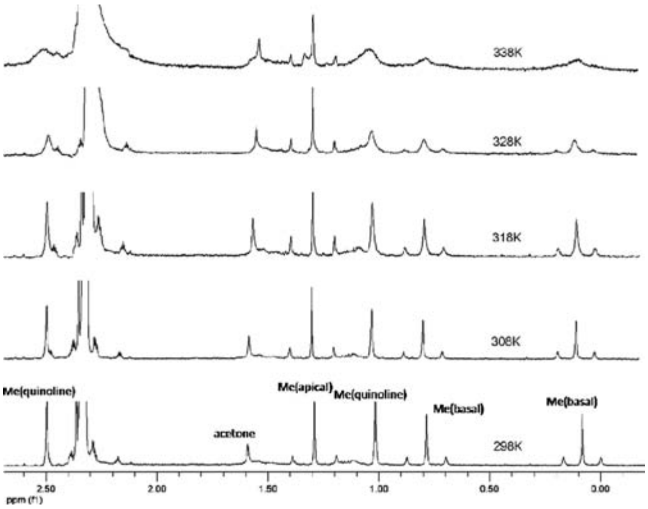

Figure 8. High-temperature ^{1}H NMR spectra of **3d** (toluene-d_8, 400 MHz). Aromatic region was omitted for clarity.

from the reaction between **1c** and $[PtMe_3OTf]_4$ in a 4:1 ratio. At ambient temperature, the ^{1}H NMR spectrum of **3c** in $CDCl_3$ shows three singlets with platinum satellites and two singlets from the quioline−methyl groups in the aliphatic region and two sets of quinoline and thiophene signals in the aromatic region, indicating an unsymmetrical structure in solution as we designed.

Attempts to obtain X-ray-quality crystals of **3c** always resulted in polycrystalline solids that were not suitable for single-crystal X-ray diffraction analyses. Therefore, a simple salt metathesis reaction between **3c** and $NaBAr^{F}_4$ was carried out to obtain a better crystal without altering the Pt-containing core structure. After stirring a 1:1 ratio mixture of **3c** and $NaBAr^{F}_4$ in DCM for several hours, the ^{1}H NMR experiment indicated the quantitative formation of a new species **3d** with the asymmetric $[Pt(IV)(\mathbf{1c})Me_3]^+$ core retained. Colorless X-ray quality crystals were obtained after crystallization of the crude product. The structure of the Pt-containing complex cation is shown in Figure 7. The C25−Pt1 vector is pointing toward C2 of the thiophene ring. The Pt1−C2 distance (2.471(8) Å) is much shorter than Pt1−C3 distance (2.821(8) Å). The two quinoline−thiophene dihedral angles are ∼68.0° and ∼37.5°, respectively, which are smaller than those in **3a**, indicating that more ligand twist is needed to minimize interligand repulsions. The space-filling model **3d** (Figure 7b) clearly showed a more sterically encumbered structure, compared to that of **3a**. The steric effect is presumably the main contributor for nonfluxional solution behavior of **3c**/**3d** at room temperature.

Investigation of the Isomerization Process. Although **3d** shows no fluxionality in solution at room temperature, because of the large isomerization barrier, high-temperature NMR spectra of **3d** show that the basal methyl proton resonances are considerably broadened while the apical methyl proton resonance remains relatively sharp up to 65 °C (Figure 8), suggesting that the interconversion of the two enantiomers through the proposed ligand twisting (eq 2) can be achieved at elevated temperatures. It is worth noting that the rotational exchange of the three Pt-Me groups reported in the literature would cause broadening or coalescence of all three methyl groups. From the line-shape analysis, the $\Delta G^{\ddagger}$ of the isomerization process at 25 °C was estimated to be 18 kcal/mol for **3d** (see the Supporting Information). Attempts to observe the coalescence at higher temperatures led to extensive decomposition of the complex.

■ CONCLUSION

In summary, we have prepared a series of five-coordinate Pt(IV) alkyl complexes **3a**−**3d**, based on quinolinyl-substituted thiophenes. These complexes can be prepared either directly from Pt(IV) starting material or through the oxidation of the dinuclear Pt(II) complexes **2a**−**2c**, respectively. Complex **3a** shows chiral structure in the solid state, but the two enantiomers undergo fast interconversion in solution, even at 180 K. We have also demonstrated that the interconversion of the two enantiomers can be slowed by introducing steric bulk at the 2-position of the quinoline ring. For example, the interconversion between the enantiomers of **3d** is slow, with respect to the NMR time scale at elevated temperatures. The chirality of complexes **3a**−**3d** originates from the repulsion between the chelating ligand and the apical methyl group rather than any unsymmetrical ligand. Variable-temperature NMR experiments and density functional theory (DFT) calculations suggest a novel isomerization mode of the two enantiomers through ligand twisting around the C−C linkages between the thiophene ring and the quinoline rings.

■ ASSOCIATED CONTENT

Supporting Information. Crystallographic data for **1c**, **2c**, **3a**, and **3d** in CIF format, and line-shape analysis, and coordinates and energies of DFT optimized structures of **3a** and transition states. This material is available free of charge via the Internet at http://pubs.acs.org.

■ AUTHOR INFORMATION

Corresponding Author
*E-mail: dsong@chem.utoronto.ca.

■ ACKNOWLEDGMENT

This research is supported by grants to D.S. from the Natural Science and Engineering Research Council (NSERC) of Canada, the Canadian Foundation for Innovation, the Ontario Research Fund, and the ERA program of Ontario. R.T. is grateful for a postgraduate scholarship from the OGS program of Ontario. Prof. Ulrich Fekl is thanked for helpful discussions.

■ REFERENCES

(1) Labinger, J. A.; Bercaw, J. E. *Nature* **2002**, *417*, 507.
(2) Goldberg, K. I.; Goldman, A. S. *Activation and Functionalization of C−H Bonds*: American Chemical Society: Washington, DC, 2004.
(3) Fekl, U.; Goldberg, K. I. *Adv. Inorg. Chem.* **2003**, *54*, 259.
(4) Puddephatt, R. J. *Angew. Chem., Int. Ed.* **2002**, *41*, 261.
(5) Lersch, M.; Tilset, M. *Chem. Rev.* **2005**, *105*, 2471.
(6) Fekl, U.; Kaminsky, W.; Goldberg, K. I. *J. Am. Chem. Soc.* **2001**, *123*, 6423.
(7) Fekl, U.; Goldberg, K. I. *J. Am. Chem. Soc.* **2002**, *124*, 6804.
(8) Fekl, U.; Kaminsky, W.; Goldberg, K. I. *J. Am. Chem. Soc.* **2003**, *125*, 15286.
(9) Kloek, S. M.; Goldberg, K. I. *J. Am. Chem. Soc.* **2007**, *129*, 3460.
(10) Luedtke, A. T.; Goldberg, K. I. *Inorg. Chem.* **2007**, *46*, 8496.
(11) Karshtedt, D.; McBee, J. L.; Bell, A. T.; Tilley, T. D. *Organometallics* **2006**, *25*, 1801.
(12) Sangtrirutnugul, P.; Tilley, T. D. *Organometallics* **2008**, *27*, 2223.

(13) Zhao, S. B.; Wu, G.; Wang, S. *Organometallics* **2008**, *27*, 1030.
(14) Zhao, S. B.; Cui, Q.; Wang, S. *Organometallics* **2010**, *29*, 998.
(15) McBee, J. L.; Tilley, T. D. *Organometallics* **2009**, *28*, 3947.
(16) West, N. M.; White, P. S.; Templeton, J. L.; Nixon, J. F. *Organometallics* **2009**, *28*, 1425.
(17) Reinartz, S.; White, P. S.; Brookhart, M.; Templeton, J. L. *J. Am. Chem. Soc.* **2001**, *123*, 6425.
(18) Tan, R.; Song, D. *Inorg. Chem.* **2010**, *49*, 2026.
(19) **3b** is a viscous liquid at room temperature.
(20) Hill, G. S.; Irwin, M. J.; Levy, C. J.; Rendina, L. M.; Puddephatt, R. J. *Inorg. Synth.* **1998**, 149.
(21) Lin, N.; Yan, J.; Huang, Z.; Altier, C.; Li, M.; Carrasco, N.; Suyemoto, M.; Johnston, L.; Wang, S.; Wang, Q.; Fang, H.; Caton-Williams, J.; Wang, B. *Nucleic Acids Res.* **2007**, *35*, 1222.
(22) Apex 2 Software Package; Bruker AXS, Inc.: Madison, WI, 2008.
(23) Sheldrick, G. M. *Acta Crystallogr., Sect. A: Found. Crystallogr.* **2008**, *64*, 112.
(24) Frisch, M. J.; Trucks, G. W.; Schlegel, H. B.; Scuseria, G. E.; Robb, M. A.; Cheeseman, J. R.; Scalmani, G.; Barone, V.; Mennucci, B.; Petersson, G. A.; Nakatsuji, H.; Caricato, M.; Li, X.; Hratchian, H. P.; Izmaylov, A. F.; Bloino, J.; Zheng, G.; Sonnenberg, J. L.; Hada, M.; Ehara, M.; Toyota, K.; Fukuda, R.; Hasegawa, J.; Ishida, M.; Nakajima, T.; Honda, Y.; Kitao, O.; Nakai, H.; Vreven, T.; Montgomery, J. A. Jr.; Peralta, J. E.; Ogliaro, F.; Bearpark, M.; Heyd, J. J.; Brothers, E.; Kudin, K. N.; Staroverov, V. N.; Keith, T.; Kobayashi, R.; Normand, J.; Raghavachari, K.; Rendell, A.; Burant, J. C.; Iyengar, S. S.; Tomasi, J.; Cossi, M.; Rega, N.; Millam, J. M.; Klene, M.; Knox, J. E.; Cross, J. B.; Bakken, V.; Adamo, C.; Jaramillo, J.; Gomperts, R.; Stratmann, R. E.; Yazyev, O.; Austin, A. J.; Cammi, R.; Pomelli, C.; Ochterski, J. W.; Martin, R. L.; Morokuma, K.; Zakrzewski, V. G.; Voth, G. A.; Salvador, P.; Dannenberg, J. J.; Dapprich, S.; Daniels, A. D.; Farkas, O.; Foresman, J. B.; Ortiz, J. V.; Cioslowski, J.; Fox, D. J. Gaussian, Inc.: Wallingford CT, 2010. Gaussian 09, Revision B.01.
(25) Becke, A. D. *J. Chem. Phys.* **1993**, *98*, 5648.
(26) Lee, C.; Yang, W.; Parr, R. G. *Phys. Rev. B* **1988**, *37*, 785.
(27) Rendina, L. M.; Puddephatt, R. J. *Chem. Rev.* **1997**, *97*, 1735.
(28) Baldwin, J. C.; Kaska, W. C. *Inorg. Chem.* **1979**, *18*, 686.
(29) Seeber, G.; Tiedemann, B. E. F.; Raymond, K. N. *Top. Curr. Chem.* **2006**, *265*, 147.

NOTE ADDED AFTER ASAP PUBLICATION

This paper was published on the Web on October 12, 2011, with textual errors in the Introduction due to production error. The corrected version was reposted on October 13, 2011.